



# CHORUS

This is the accepted manuscript made available via CHORUS. The article has been published as:

## Intrinsic low thermal conductivity in weakly ionic rocksalt structures

Yi Zhang, Jianjun Dong, Paul R. C. Kent, Jihui Yang, and Changfeng Chen

Phys. Rev. B **92**, 020301 — Published 6 July 2015

DOI: [10.1103/PhysRevB.92.020301](https://doi.org/10.1103/PhysRevB.92.020301)

# Intrinsic Low Thermal Conductivity in Weakly Ionic Rocksalt Structures

Yi Zhang,<sup>1</sup> Jianjun Dong,<sup>2</sup> Paul R. C. Kent,<sup>3</sup> Jihui Yang,<sup>4</sup> and Changfeng Chen<sup>1</sup>

<sup>1</sup>*Department of Physics and HiPSEC, University of Nevada, Las Vegas, Nevada 89154*

<sup>2</sup>*Physics Department, Auburn University, Auburn, Alabama 36849*

<sup>3</sup>*Center for Nanophase Materials Sciences and Computer Science and Mathematics Division, Oak Ridge National Laboratory, Oak Ridge, Tennessee 37831*

<sup>4</sup>*Department of Materials Science, University of Washington, Seattle, Washington 98195*

(Dated: June 23, 2015)

A fundamental challenge in thermoelectric (TE) material research is meeting the simultaneous requirements of high carrier mobility and low thermal conductivity. Simple crystal structures are ideal for maintaining high carrier mobility, but they usually have high thermal conductivity. Here we show by first-principles lattice dynamics and Boltzmann transport calculations that weakly ionic rocksalt (RS) structures exhibit strong lattice anharmonicity and low acoustic-phonon group velocity, which combine to produce intrinsic low thermal conductivity. We unveil microscopic mechanisms that explain experimental observations and provide insights for new TE material design and discovery.

PACS numbers: 63.20.-e, 72.15.Jf, 71.20.-b

Thermoelectric (TE) materials hold great promise for clean energy applications [1, 2], but they present a fundamental challenge in simultaneously requiring high electrical but low thermal conduction. Most recent work focused on reducing lattice thermal conductivity ( $\kappa_L$ ) via phonon scattering by complex microstructural features, such as superlattice interfaces, grain boundaries, caged dopants, etc. [3–8]. Semiconductors in simple crystal structures are best suited to maintain high carrier mobility, but they usually exhibit high  $\kappa_L$ . There are, however, exceptions, most notably the IV-VI (PbTe, PbSe, PbS) compounds in rocksalt (RS) structure with  $\kappa_L$  below 2.5 W/mK at room temperature, which is comparable to that of complex TE materials [6]. This unusual behavior has been attributed to giant anharmonic phonon coupling [9], ferroelectric instability [10, 11], lone-pair electrons [12], or spontaneous nanostructuring [13]. Nevertheless, an understanding of the fundamental mechanisms still requires a thorough examination of the underlying lattice dynamics and phonon scattering processes, which has been the focus of recent efforts, including the development of codes like the ShengBTE package [14].

In crystalline materials, heat is mostly carried by long-lifetime acoustic phonon. At a microscopic level,  $\kappa_L$  depends on phonon group velocity  $v_g$  and lifetime  $\tau$ . Weak acoustic phonon dispersions produce low  $\kappa_L$  in superlattice and Van der Waals systems [15, 16]. Simple cubic structures are inherently unstable because the nearest-neighbor interactions do not contribute to  $C_{44}$  shear modulus, whereas the next-nearest neighbors may contribute negatively [17]. This tendency of structural instability strongly impacts acoustic phonon dispersion and  $v_g$ . In this work, we show that low acoustic-phonon  $v_g$  and strong anharmonicity in select weakly ionic RS compounds combine to produce extremely low  $\kappa_L$ . Our results explain intriguing low thermal conduction observed in several RS structure TE materials. Since many semi-

conductor compounds, solid solutions, and nanocomposites adopt RS structure, our work may open a promising new avenue for discovery of low  $\kappa_L$  TE materials.

We performed first-principles calculations using the VASP code [18] within the generalized gradient approximation (GGA-PBE) [19] and the projector augmented wave (PAW) [20] method with a cutoff energy of 400 eV. Scalar relativistic effects and spin-orbit interaction (SOI) were included as needed. We calculated lattice thermal conductivity based on the relaxation time approximation of the phonon gas using the formula  $\kappa_L = \frac{1}{3} \sum_{\mathbf{q}s} C_{\mathbf{q}s} v_{g,\mathbf{q}s}^2 \tau_{\mathbf{q}s}$ , where  $C_{\mathbf{q}s}$ ,  $v_{g,\mathbf{q}s}$ , and  $\tau_{\mathbf{q}s}$  are specific heat, group velocity, and lifetime of phonon mode with momentum  $\mathbf{q}$  and polarization index  $i$ , respectively. We performed harmonic lattice dynamics calculations using fpho [21] and our own codes to derive heat capacity and group velocity. Phonon lifetime  $\tau$  is inversely proportional to phonon scattering rate  $\Gamma_{\mathbf{q}s}$  given by

$$\begin{aligned} \Gamma_{\mathbf{q}s} = & \sum_{s's''} \frac{\hbar\pi}{16} \int_{BZ} |A_{ss's''}^{\mathbf{q}\mathbf{q}'\mathbf{q}''}|^2 \Delta_{\mathbf{q}\mathbf{q}'\mathbf{q}''} \times \\ & [(n_{\mathbf{q}'s'} + n_{\mathbf{q}''s''} + 1)\delta(\omega_{\mathbf{q}s} - \omega_{\mathbf{q}'s'} - \omega_{\mathbf{q}''s''}) \\ & + 2(n_{\mathbf{q}'s'} - n_{\mathbf{q}''s''})\delta(\omega_{\mathbf{q}s} - \omega_{\mathbf{q}'s'} + \omega_{\mathbf{q}''s''})] d\mathbf{q}d\mathbf{q}''. \end{aligned} \quad (1)$$

Here  $n_{\mathbf{q}s}$  is the phonon occupation number in the Bose-Einstein distribution,  $\Delta_{\mathbf{q}\mathbf{q}'\mathbf{q}''}$  ensures the momentum conservation  $\mathbf{q} + \mathbf{q}' + \mathbf{q}'' = \mathbf{G}$  and the delta functions ensure energy conservation. The three-phonon matrix elements are obtained from

$$\begin{aligned} A_{ss's''}^{\mathbf{q}\mathbf{q}'\mathbf{q}''} = & \sum_{ijk} \sum_{\alpha\beta\gamma} \frac{\epsilon_{\alpha i}^{\mathbf{q}s} \epsilon_{\beta j}^{\mathbf{q}'s'} \epsilon_{\gamma k}^{\mathbf{q}''s''}}{\sqrt{m_i m_j m_k} \sqrt{\omega_{\mathbf{q}s} \omega_{\mathbf{q}'s'} \omega_{\mathbf{q}''s''}}} \times \\ & \Psi_{ijk}^{\alpha\beta\gamma} e^{i(\mathbf{q}\cdot\mathbf{r}_1 + \mathbf{q}'\cdot\mathbf{r}_2 + \mathbf{q}''\cdot\mathbf{r}_3)}, \end{aligned} \quad (2)$$

where  $m_i$  is the atomic mass, and  $\epsilon^{\mathbf{q}s}$  is the phonon polarization vector. The third order interatomic force constants (IFCs)  $\Psi$  are calculated by taking the derivative of

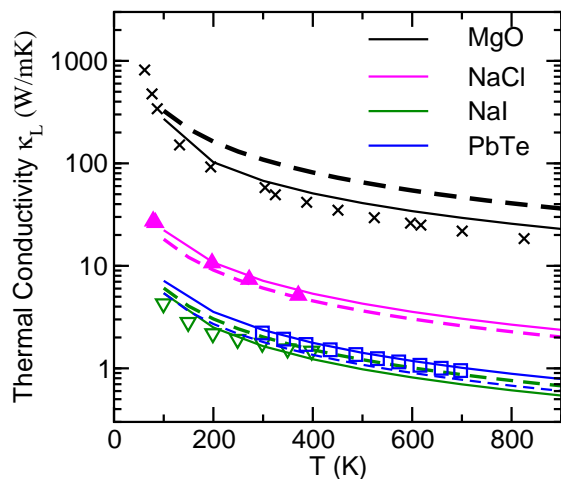


FIG. 1: (Color Online) Calculated lattice thermal conductivity versus temperature for MgO, NaCl, NaI, and PbTe. Solid and dashed lines are results of first-principles calculations and Slack's model [Eq. (3)] [25], respectively. Also shown are experimental  $\kappa_L$  for MgO (cross) [26, 27], NaCl (up-triangle) [28], NaI (down-triangle) [29], and PbTe (square) [30].

the second-order IFCs using the finite difference method; because all the major third-order IFCs are between the first- and second-nearest-neighbors, pair interactions beyond the second-nearest neighbors are set to zero. This procedure treats the lattice anharmonicity, allowing its incorporation into the computational codes [14, 22, 23]. Translational invariance of the third-order IFCs is imposed using a  $\chi^2$  minimization technique [24].

Using the first-principles approach we have calculated intrinsic lattice thermal conductivity of MgO, NaCl, NaI, and PbTe. The results (Fig. 1) agree well with experimental data. These compounds exhibit remarkable disparity in  $\kappa_L$  at room temperature (300 K): NaI has a  $\kappa_L$  of only 1.64 W/mK, an extremely low value for a material in a simple crystal structure; PbTe has a slightly higher  $\kappa_L$  of 2.36 W/mK despite its much larger atomic mass; NaCl and MgO, which are much lighter than PbTe, exhibit considerably higher  $\kappa_L$  of 7.12 and 67.6 W/mK, respectively. To analyze factors that influence  $\kappa_L$ , we use Slack's model [25], which gives

$$\kappa_L = A \frac{\bar{M} \theta_D^3 \delta}{\gamma^2 n^{2/3} T}, \quad (3)$$

where  $n$  is the number of atoms in the primitive cell,  $\delta^3$  is the volume per atom,  $\theta_D$  is the Debye temperature,  $\bar{M}$  is the average atomic mass,  $\gamma$  is the high temperature limit of the acoustic phonon Grüneisen parameter, and  $A$  represents a collection of physical constants that depends on  $\gamma$ . From the average frequency change of acoustic modes with respect to volume change we obtained large  $\gamma$  values of 1.552, 1.314, and 1.315 for MgO, NaCl, and NaI, respectively. The SOI has a strong effect on the value

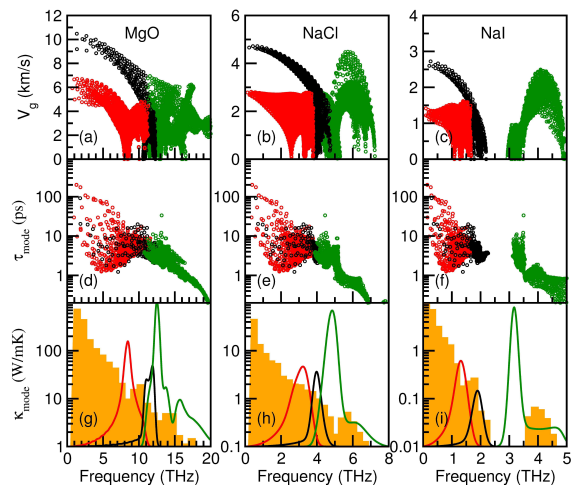


FIG. 2: (Color Online) (a-c) Frequency-dependent phonon velocity  $v_g$ , (d-f) lifetime  $\tau$ , and (g-i) thermal conductivity  $\kappa_L$  for MgO, NaCl, and NaI. Open circles in red, black, and green in (a)-(f) represent TA, LA, and optic phonon data, respectively. Red, black, and green lines in (g)-(i) are normalized phonon density of states of the TA, LA, and optic phonon modes in arbitrary units. The yellow semi-log histogram plots in (g)-(i) are averaged mode  $\kappa_L$  at different frequencies with the interval of 0.9, 0.3, and 0.2 THz for MgO, NaCl, and NaI, respectively.

of  $\gamma$  for PbTe. Our SOI calculations for PbTe produced  $\gamma = 1.584$ , which is significantly smaller than  $\gamma = 2.066$  from non-SOI calculations and is consistent with previously reported data [25]. We have also examined other RS structure compounds, such as AgCl, BaO, BrI, and CdO, and the obtained  $\gamma$  values consistently fall between 1.3 to 1.6 despite large differences in charge, volume, and mass density. These  $\gamma$  values are well above the 0.5-1.0 range for typical thermoelectric materials [25], and they show a general trend of strong lattice anharmonicity in this class of materials in RS structure, which may be related to the central force nature of ionic interactions [31]. The strong anharmonicity, however, has little effect on the large disparity of  $\kappa_L$  since the  $\gamma$  values of these materials all fall into a narrow range. We then evaluated the Debye temperature by fitting the low-temperature heat capacity to the Debye model, and obtained  $\theta_D$  of 973, 277, 120, and 108 K for MgO, NaCl, NaI, and PbTe, respectively. Low Debye temperature is known to be related to short phonon lifetime [32]. This large variation of Debye temperature is mainly responsible for the large  $\kappa_L$  disparity since  $\theta_D$  contributes cubically to  $\kappa_L$ . It is noted (see Fig. 1) that the  $\kappa_L$  values for NaCl, NaI, and PbTe obtained from Eq. (3) are in good agreement with the results of our three-phonon scattering calculations and experimental data, but for MgO, which has a much higher  $\theta_D$ , the high-temperature Slack model is less accurate in the temperature range studied here.

To unveil microscopic phonon transport mechanisms,

we calculated the frequency dependent phonon mode  $v_g$ . The results for MgO, NaCl, and NaI are shown in Fig. 2. In harmonic lattice dynamics, low  $v_g$  shares the same origin that produces low  $\theta_D$ , such as heavy average atomic mass and weak interatomic bonding. The ionic bond in MgO by its formal charge state is four times as strong as that in NaCl and NaI at the same bond length. The stronger Coulomb attraction further reduces the interatomic distance and enhances the bonding strength in MgO. As a result, the  $v_g$  for MgO is substantially larger than those for NaCl and NaI. NaI has the same ionic charge as NaCl, but it is three times heavier than NaCl and its calculated lattice parameter is 15% larger. Thus, the  $v_g$  of NaI is lower than that of NaCl. The same RS structure of these compounds leads to similar frequency dependence of their acoustic phonon  $v_g$  and  $\tau$ . The LA phonon  $v_g$  peaks at the Brillouin zone center and decreases to zero at the zone boundary. The TA phonon follows the same trend but the  $v_g$  is much lower. For NaI, the long-wave TA  $v_g$  along  $\Gamma - L$  [001] is 1485 m/s, which is comparable to the sound velocity in solid argon [16]. Meanwhile, the TA  $v_g$  for MgO and NaCl are 6562 and 2868 m/s, respectively. The  $\tau$  values for acoustic phonon are in general an order of magnitude larger than those of optic phonon, which is consistent with the frequency dependence of  $\kappa_L$ . This shows that the low frequency acoustic phonon is the dominant heat carrier. The much lower  $v_g$  of NaI produces its frequency dependent  $\kappa_L$  that is nearly two orders of magnitude smaller than that of MgO. It shows that the weak ionic charge in NaI has a significant effect on reducing its acoustic phonon  $v_g$ , leading to the extremely low  $\kappa_L$ .

In many octet semiconductors, the covalent fourfold coordinated zinc-blend structure competes with the ionic sixfold coordinated RS structure. For weakly ionic crystals, covalent bonding character dominates the nearest-neighbor interactions. However, as illustrated in Fig. 3(a), the RS structure tends to develop a shear-type transversal acoustic (TA) softening along  $\Gamma - X$ , which is an intrinsic incipient instability. To evaluate such TA softening and the associated  $v_g$  change, we employ the rigid ion model for partially ionic RS structures where the long-range interactions that stabilize the RS structure depend on the effective ionic charge ( $Z$ ), which can be significantly smaller than the nominal charge in weakly ionic crystals [33]. We treat the second-order bond stretching force constants between nearest neighbors as constant for different  $Z$ , since they are dominated by the directional covalent interactions. For simplicity, we adopt the atomic mass ratio 2:1 and set the lattice constant and unit atomic mass to unity. The dispersion and  $v_g$  of the lower TA (TA1) branch is shown in Fig. 3(b). As  $Z$  decreases from 1.5 to 0.5, there is a broad softening of the TA1 branch along high symmetry  $k$ -lines except the  $\Gamma - L$  [111], where phonon vibration is associated with bond compression and stretching that are dominated by

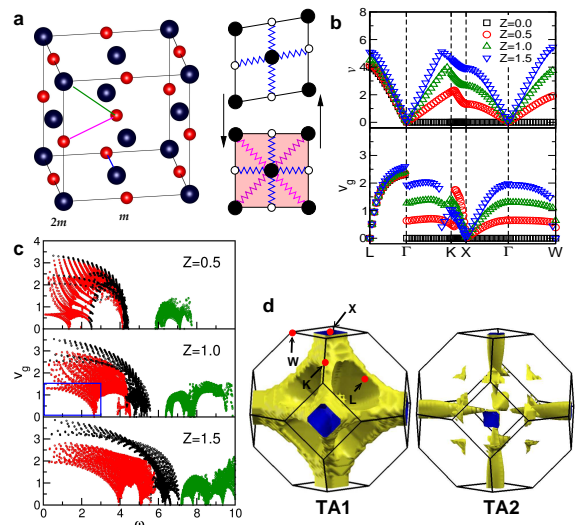


FIG. 3: (Color Online) (a) Illustration of incipient shear instability in RS structure. (b) Simulated TA phonon dispersion and  $v_g$  for ionic RS structures with different effective ionic charge  $Z$ . The RS structure is unstable when  $Z=0$  in the absence of Coulomb interaction. (c) Frequency dependent  $v_g$  of TA (red), LA (green), and optic (black) phonon at different  $Z$ . (d) The distribution of the low-frequency low- $v_g$  data from the region marked by the blue square in (c) at  $Z = 1$  in the first Brillouin zone.

the covalent bonding character. As a result, the  $v_g$  of the TA1 branch decreases with decreasing  $Z$  when the phonon dispersion becomes flat. The higher TA branch (TA2) coincides with the TA1 branch along the [001] and [111] directions. In other  $k$ -lines, the  $v_g$  of TA2 also decreases with decreasing  $Z$  but at a slower rate. Fig. 3(c) shows the frequency dependent  $v_g$ . We are primarily interested in the low frequency acoustic phonon modes since they have the longest  $\tau$ . The TA  $v_g$  diverges significantly with decreasing  $Z$  below  $\omega = 2$ , leading to more TA phonon modes in the low  $v_g$  region, which substantially impedes the heat conduction ability of TA phonon near the  $\Gamma - X$  line (TA1 and TA2) and the plane between  $\Gamma - X$  and  $\Gamma - K$  lines (TA1) [see Fig. 3(d)].

Recent studies show that, despite its nominal ionic charge of 2.0, PbTe is only weakly ionic with an effective ionic charge of 0.72 [11, 34]. This is consistent with the observation that the TA phonon of PbTe shows significantly diverging  $v_g$  at low frequencies [Fig. 4(a)], which corresponds to the low- $Z$  case of the model calculations [Fig. 3(c)]. We select two representative directions, [001] and [111], to illustrate the different frequency and  $v_g$  behavior of the TA phonon relative to that of the LA phonon [see Fig. 4(b-g)]. The TA branch is very soft compared to the LA branch in the [001] direction. The LA phonon frequency is 3.3-3.5 times as large as that of TA phonon near the zone center. In comparison, the LA-to-TA frequency ratio is smaller than 2 for MgO, NaCl, and NaI. The weak TA phonon dispersion of PbTe leads

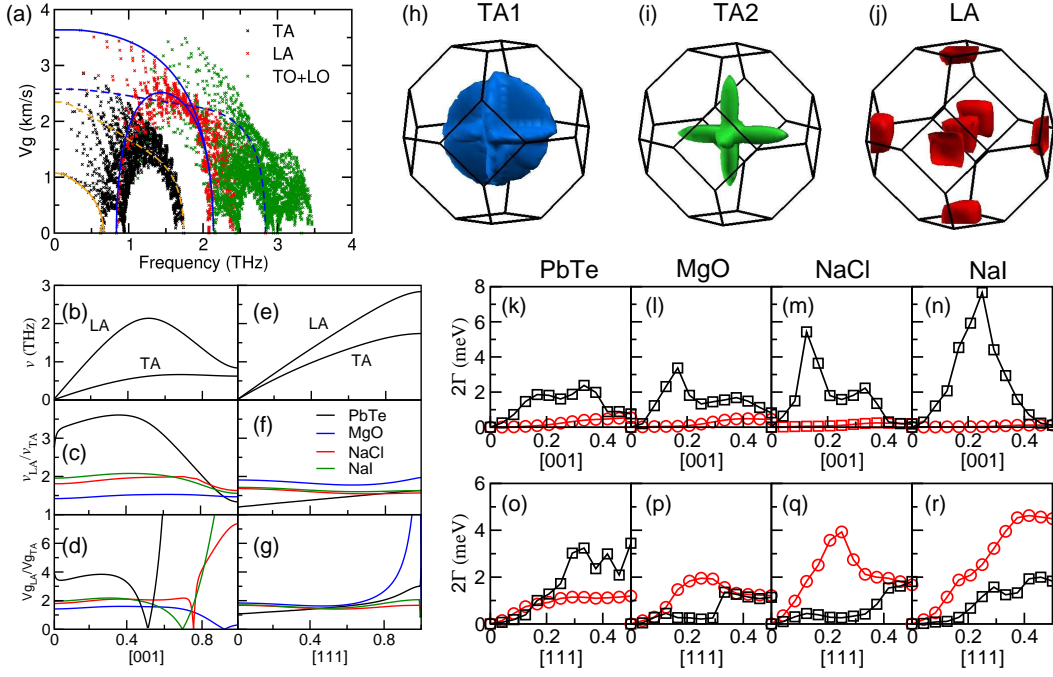


FIG. 4: (Color Online) (a) Frequency dependent  $v_g$  of PbTe. The TA (solid lines) and LA (dash lines) branches along  $\Gamma - X$  [001] and  $\Gamma - L$  [111] are in yellow and blue, respectively. (b)-(g) The dispersion and frequency and  $v_g$  ratio of the LA to TA phonon branch of PbTe along the [001] and [111] directions compared with data for MgO, NaCl, and NaI. (h)-(j) The distribution of the long-lifetime TA1 (lower TA), TA2 (higher TA), and LA phonon branches of PbTe with  $\tau$  greater than 10, 10, and 4 ps, respectively. (k)-(r) The linewidths ( $2\Gamma = \tau^{-1}$ ) of the TA (black) and LA (red) phonon along the [001] and [111] directions for PbTe, MgO, NaCl, and NaI.

to a  $v_g$  of 1064 m/s at the long-wave limit, which is even lower than the corresponding TA  $v_g$  of NaI. We also obtain a large  $v_g(LA)/v_g(TA)$  ratio of 3.42 for PbTe in the long-wave limit, compared to 1.41, 1.81, 1.96 for MgO, NaCl, and NaI, respectively. In the [111] direction, the TA vibrations are associated with both bond stretching and torsion. As a result, the TA branch is elevated by the covalent character of the Pb-Te bond, and the frequency and  $v_g$  disparity between the LA and TA branches is smaller than that in highly ionic RS systems.

To probe the correlation between the acoustic phonon  $v_g$  profile and  $\kappa_L$ , we examine the distribution of long-lifetime acoustic phonon in the k-space (first Brillouin zone). As shown in Fig. 4(h-i), the longest lifetime ( $\tau > 10$  ps) TA phonon has considerable overlap with the low  $v_g$  TA phonon [see Fig. 3(d)] around the [001] direction, indicating that low  $v_g$  of the [001] TA phonon is a major limiting factor of the TA thermal conductivity in PbTe. The LA phonon is not significantly affected by the weak ionic charge of PbTe. Instead, they maintain high  $v_g$  in the zone center and the neighboring low frequency region. The low LA thermal conductivity of PbTe can be attributed to the  $\tau$  of the LA phonon, which is in general shorter than that of the TA phonon. As shown in Fig. 4(j), the LA phonon with  $\tau > 2$  ps is distributed around the zone center and the X point. Previous studies show that the  $\tau$  of the [001] LA phonon is short due to

the strong coupling between the LA and transverse optic phonon in PbTe [9, 35]. This finding is in agreement with the calculated LA phonon linewidth shown in Fig. 4(k). Interestingly, we obtain even larger [001] peak linewidths for LA phonon in MgO, NaCl, and NaI [see Fig.4 (l-n)], which suggests a similar origin of strong [001] LA phonon scattering in these materials. In the [111] direction, the LA phonon of PbTe has larger linewidths than those of MgO, NaCl, and NaI, which again suggests low LA thermal conductivity in PbTe.

In summary, we have examined lattice thermal conductivity of materials in RS structure using first-principles lattice dynamics and Boltzmann transport calculations. We identify effective ionic charge as a critical parameter that influences heat transport in these materials. Weakly ionic RS structures exhibit strong lattice anharmonicity and low acoustic phonon group velocity, leading to extremely low lattice thermal conductivity in select RS crystals like PbTe and NaI. The present work offers new insights into the anharmonic phonon scattering and heat transport at a microscopic level, which improve the fundamental understanding of experimentally observed intrinsic low thermal conductivity in RS crystals. More important, they also suggest a new design strategy of tuning the ionicity of RS crystals to reduce lattice thermal conduction, which may open new opportunities for discovery of advanced thermoelectric materials.

This work is supported by DOE through Cooperative Agreement DE-NA0001982. Research by PRCK was conducted at the Center for Nanophase Materials Sciences, which is sponsored at Oak Ridge National Laboratory by the Scientific User Facilities Division, Office of Basic Energy Sciences, U.S. Department of Energy.

- 
- [1] H. J. Goldsmid, *Thermoelectric Refrigeration* (Plenum, New York, 1964).
- [2] L. E. Bell, *Science* **321**, 1457 (2008).
- [3] G. J. Snyder and E. S. Toberer, *Nature Mater.* **7**, 105 (2008).
- [4] M. G. Kanatzidis, *Chem. Mater.* **22**, 648 (2010).
- [5] T. C. Harman, P. J. Taylor, M. P. Walsh, and B. E. LaForge, *Science* **297**, 2229 (2002).
- [6] B. C. Sales, D. Mandrus, and R. K. Williams, *Science* **272**, 1325 (1996).
- [7] G. S. Nolas, J. L. Cohn, G. A. Slack, and S. B. Schujman, *Appl. Phys. Lett.* **73**, 178 (1998).
- [8] H. Liu, X. Shi, F. Xu, L. Zhang, W. Zhang, L. Chen, Q. Li, C. Uher, T. Day, and G. J. Snyder, *Nature Mater.* **11**, 422 (2012).
- [9] O. Delaire, K. Ma, K. Marty, A. F. May, M. A. McGuire, M. H. Du, D. J. Singh, A. Podlesnyak, G. Ehlers, M. D. Lumsden, and B. C. Sales, *Nature Mater.* **10**, 614 (2011).
- [10] E. S. Božin, C. D. Malliakas, P. Souvatzis, T. Proffen, N. A. Spaldin, M. G. Kanatzidis, S. J. L. Billinge, *Science* **330**, 1660 (2010).
- [11] Y. Zhang, X. Ke, P. R. C. Kent, J. Yang, and C. Chen, *Phys. Rev. Lett.* **107**, 175503 (2011).
- [12] D. T. Morelli, V. Jovovic, and J. P. Heremans, *Phys. Rev. Lett.* **101**, 035901 (2008).
- [13] J. Ma, O. Delaire, A. F. May, C. E. Carlton, M. A. McGuire, L. H. VanBebber, D. L. Abernathy, G. Ehlers, T. Hong, A. Huq, W. Tian, V. M. Keppens, Y. Shao-Horn, and B. C. Sales, *Nature Nanotech.* **8**, 445 (2013).
- [14] W. Li, L. Lindsay, D. A. Broido, D. A. Stewart, and N. Mingo, *Phys. Rev. B* **86**, 174307 (2012).
- [15] A. Balandin and K. L. Wang, *J. Appl. Phys.* **84**, 6149 (1998).
- [16] G. J. Keeler and D. N. Batchelder, *J. Phys. C* **3**, 510 (1970).
- [17] M. Born and K. Huang, *Dynamical Theory of Crystal Lattices* Clarendon, Oxford, (1954).
- [18] G. Kresse and J. Furthmüller, *Phys. Rev. B* **54**, 11169 (1996).
- [19] J. P. Perdew, K. Burke, and M. Ernzerhof, *Phys. Rev. Lett.* **77**, 3865 (1996).
- [20] G. Kresse and D. Joubert, *Phys. Rev. B* **59**, 1758 (1999).
- [21] A. Togo, F. Oba, and I. Tanaka, *Phys. Rev. B* **78**, 134106 (2008).
- [22] X. Tang and J. Dong, *Proc. Natl. Acad. Sci. USA* **107**, 4539 (2009).
- [23] K. Esfarjani, G. Chen, and H. T. Stokes, *Phys. Rev. B* **84**, 085204 (2011).
- [24] L. Lindsay, D. A. Broido, and T. L. Reinecke, *Phys. Rev. B* **87**, 165201 (2013).
- [25] D. T. Morelli and G. A. Slack, "High Thermal Conductivity Materials" edited by S. L. Shindé and J. S. Goela, Springer page 37-68 (2006).
- [26] G. A. Slack, *Phys. Rev.* **126**, 472 (1962).
- [27] H. Kanamori, N. Fujii, and H. Mizutani, *J. Geophys. Res.* **73**, 595 (1968).
- [28] A. Eucken, *Ann. Physik* **34**, 185 (1911).
- [29] E. D. Devyatkova and I. A. Smirnov, *Sov. Phys.-Solid State* **4**, 1836 (1963).
- [30] V.I. Fedorov, V.I. Machuev, *Sov. Phys. Solid State USSR* **11**, 1116 (1969).
- [31] A. Chernatynskiy, J. E. Turney, A. J. H. McGaughey, C. H. Amon, and S. R. Phillpot, *J. Am. Ceram. Soc.* **94**, 3523 (2011).
- [32] W. Li and N. Mingo, *Phys. Rev. B* **90**, 094302 (2014); *ibid.* **89**, 184304 (2014).
- [33] J. C. Phillips, *Rev. Mod. Phys.* **42**, 317 (1970).
- [34] H. Kim and M. Kaviani, *Phys. Rev. B* **86**, 045213 (2012).
- [35] T. Shiga, J. Shiomi, J. Ma, O. Delaire, T. Radzyski, A. Lusakowski, K. Esfarjani, and G. Chen, *Phys. Rev. B* **85**, 155203 (2012).